Magnetic Microactuation of Polysilicon Flexure Structures

Jack W. Judy, Richard S. Muller, and Hans H. Zappe

Berkeley Sensor & Actuator Center (BSAC)
Department of EECS, University of California
Berkeley, California 94709

***Abstract-*A novel microactuator technology that combines magnetic thin films with polysilicon flexural structures is described. Devices are constructed in a batch-fabrication process which combines electroplating with conventional lithography, materials, and equipment. A microactuator consisting of a 400x(47-40)x7 μm^3 rectangular plate of NiFe attached to a 400x(0.9-1.4)x2.25 μm^3 polysilicon beam has been displaced over 1.2 mm, rotated over 180°, and actuated with over 0.185 nNm of torque. Theoretical expressions for the displacement and torque are developed and compared to experimental results.**

I. INTRODUCTION

MAGNETIC microactuation has recently been demonstrated by several research groups [1-5]. In most cases magnetic-microactuator fabrication is not accomplished in a continuous batch process, but rather with the addition of steps such as manual assembly. The cantilever actuator described by Ahn and Allen is an exception [3]. In our paper, we describe batch-fabricated magnetic microactuators which are made in a relatively simple process. This process combines electroplated NiFe films with surface-micromachined polycrystalline silicon. This combination of materials provides new opportunities for actuated-structure designs. Specifically, forces and displacements that are larger than those generated with electrostatic microactuators are readily obtained. An important feature of this technology is provided by the ability to control the actuators via a remote source for the magnetic field. This type of control can achieve significant actuation both in and out of the plane of the wafer. These advantages of magnetic drive can accelerate and broaden the already impressive results obtained with actuated polysilicon microflexural elements [6-8]. Full integration of magnetically actuated elements into microsystems can be expected to have significant impact. There appears to be no major obstacle to the merger of electrical, mechanical, and magnetic microfabrication technologies.

II. TECHNOLOGY

The new microactuators are produced by adding fabrication steps to a process developed at BSAC to produce polysilicon surface-parallel microresonant systems [9]. All steps are added near the end of the fabrication sequence, just prior to the micromechanical-device "release" step. This processing sequence avoids contamination by the magnetic material during the conventional microelectronic and micromechanical fabrication steps.

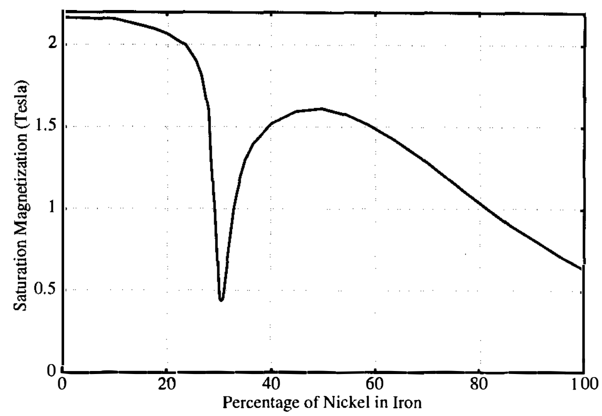

Fig. 1. The saturation magnetization of a NiFe film as a function of composition. (*Based on Bozorth* [10])

Furthermore, no additional step adds significantly to the thermal budget for the wafer.

The micromechanical flexures are constructed with phosphorus-doped LPCVD polysilicon. An electroplated nickel-iron alloy is used as the magnetic material because of its relatively high saturation magnetization. In addition, the magnetic properties of NiFe have been well-documented because of its very widespread commercial use. The NiFe is electroplated by using a variation of a procedure described by Ahn, Kim, and Allen [4]. For magnetic thin-film heads, one normally seeks to control the film composition at 81% Ni, 19% Fe in order to eliminate stress-induced magnetic anisotropy. Plating control to achieve a given composition is challenging, however, and our films turned out to be rich in nickel -- roughly 95% Ni and 5% Fe as measured by an energy-dispersive, x-ray microanalysis system mounted in a scanning-electron microscope [11]. On the other hand, to maximize actuation performance the saturation magnetization should be maximized. For a NiFe film this occurs at a composition of 100% Fe. Unfortunately, iron corrodes easily and thus it is beneficial to add nickel which is much more corrosion resistant. A composition of 50% nickel provides improved corrosion resistance and corresponds to a local maximum of the saturation magnetization (Figure 1). A nickel-iron alloy with 50% nickel and 50% iron has historically been referred to as 50 Permalloy [12]. A design concern for non-released structures made with 50 Permalloy is that the magnetostriction is much higher at 50% nickel (~2.6×10^{-5}) than at 81% nickel (~0). Thus, unless the stress in the magnetic film can be relaxed (for example, in this work in which the magnetic element can move freely) there may be significant mechanical effects on the magnetic properties.

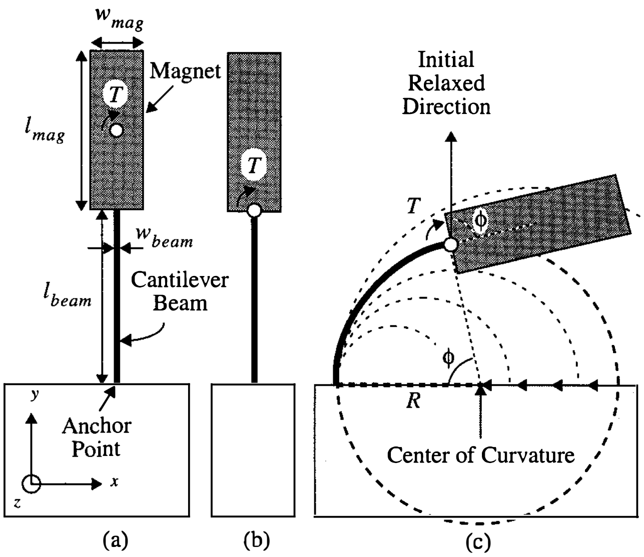

Fig. 2. (a) Mechanical structure of the microactuator. (b) Reduction of the mechanical system. (c) Circular beam bending. The arrows indicate the motion of the center of curvature as T is increased from zero.

III. MECHANICAL ANALYSIS

For a first microactuated element, we built and studied the structure shown in Fig. 2a. It consists of a narrow cantilever beam made of polysilicon which is anchored to the substrate at one end and attached to a wide plate of magnetic material at the other end. When the long and thin magnetic plate is placed in a uniform magnetic field it experiences only a pure moment and not a translational force. Since the magnetic material is much wider, thicker, and stiffer than the cantilever beam, the magnetic material can be assumed to be mechanically rigid. To simplify the analysis, we recognize that a pure moment applied to a rigid body can be translated to any position on the rigid body. Therefore, the resulting mechanical model becomes that of a simple cantilever beam which is fixed at one end and has a concentrated moment or torque T applied to the other end (Fig. 2b).

If we assume that the cantilever beam has a uniform cross section, the application of a torque results in pure bending. Thus, increasing the magnetic field H configures the beam along the path of a circular arc, whose center translates in from infinity along the anchoring surface (Fig. 2c). In terms of the torque T on the plate, the radius of curvature R of the cantilever beam is given by

$$R = \frac{l_{beam}}{\phi} = \frac{E_Y I}{T} \qquad (1)$$

with cantilever-beam length l_{beam}, elastic modulus E_Y, and moment-of-inertia I [13]. The angle ϕ is the angular mechanical deflection from the initial relaxed direction.

The fabrication process that forms the polysilicon beam produces a trapezoidal cross section. Using the moment-of-inertia of a beam with a trapezoidal cross section [14], the angular deflection in Eq. (1) can be expressed as

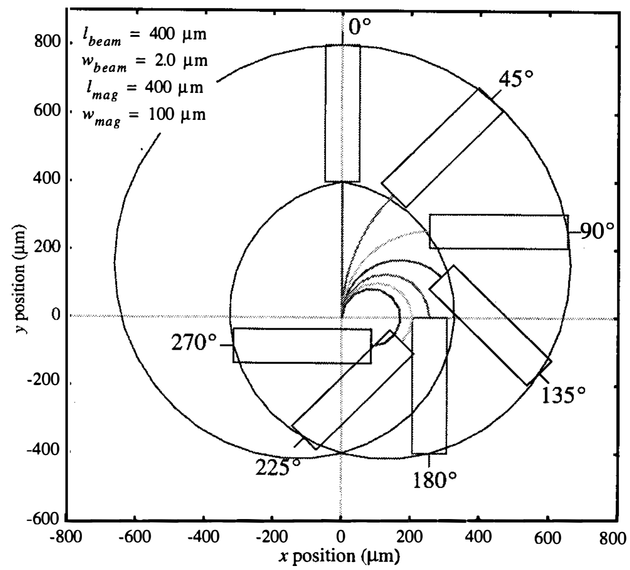

Fig. 3. Plot of the deflection of the end of the microactuator. The cardioid traces out the position of the tip as the angular deflection of the plate ϕ is increased by increasing the torque T. The resulting deformed shape is shown for angular deflections of ϕ = 0, 45, 90, 135, 180, 225 and 270°.

$$\phi = \frac{48\, T\, l_{beam}}{E_Y h\,(a+b)\left(a^2+b^2\right)} = \frac{T}{k_\phi} \qquad (2)$$

with beam thickness h, upper-beam width a, and lower-beam width b. Equation (2) is useful for determining the torque T from observation of the angular mechanical deflection ϕ. The angular spring constant k_ϕ of this mechanical structure is given by

$$k_\phi = \frac{E_Y h\,(a+b)\left(a^2+b^2\right)}{48\, l_{beam}} \qquad (3)$$

Equations (1) to (3) assume Hooke's-law behavior for the cantilever material.

A. Description of Motion

Coordinates for the position of the tip of the actuated cantilever can be obtained from a straightforward geometrical analysis. The results, given in Eqns. (4) and (5), are plotted in Fig. 3.

$$x_{tip} = \frac{l_{beam}}{\phi}(1-\cos\phi) + l_{mag}\sin\phi \qquad (4)$$

$$y_{tip} = \frac{l_{beam}}{\phi}\sin\phi + l_{mag}\cos\phi \qquad (5)$$

Figure 3 is a plot of the path traced out by the tip of a microactuator with a cantilever beam of length l_{beam} = 400 µm and a rigid magnetic plate of length l_{mag} = 400 µm. To achieve these large deflections the moment is increased by varying the magnetic-field intensity and direction. The largest x-translation of the tip is

$$x_{max} \approx \pm\left(\frac{2}{\pi} l_{beam} + l_{mag}\right) = \pm 654\ \mu\text{m} \qquad (6)$$

and the largest y-translation of the tip is

$$y_{max} \approx -(2 l_{mag} + l_{beam}) = -1200\ \mu\text{m} \qquad (7)$$

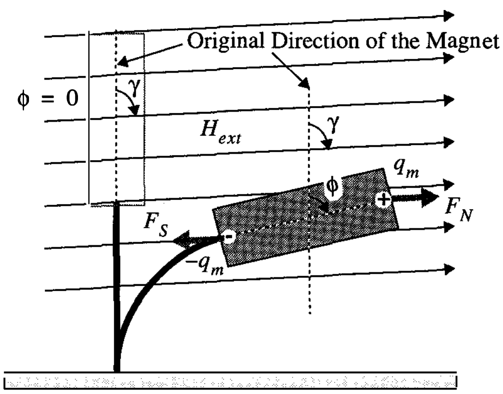

Fig. 4. Positions of the effective magnetic "charges" and directions of the forces that they generate. The angular mechanical deflection ϕ and the angle between the magnetic field and the original direction of the cantilever structure γ are also labeled.

IV. MAGNETIC ANALYSIS

The behavior of long and narrow magnets in a magnetic field can be modeled using the concept of "effective magnetic charges." Although no magnetic monopoles exist, these effective magnetic charges are formed in pairs and they are mathematically identical to electrical charges. To generate a useful picture of the magnetic-field pattern, one can postulate that positive magnetic charges reside on the magnetic north pole and negative magnetic charges reside on the magnetic south pole. In Fig. 4, we use this concept to introduce magnetic charges q_m and $-q_m$ to the cantilever actuator.

Since, to first order, we assume the magnetic material is uniformly magnetized, the magnetic charges exist only on the very ends of the magnet. The charges, which are separated by the length of the magnet, experience the forces $F_N = q_m H_{ext}$ and $F_S = -q_m H_{ext}$. These forces line up with the external field lines (Fig. 4). The angle between the original direction of the magnet and the direction of the magnetic field is γ. To deflect the structure by an angle ϕ, the magnetic-field direction is held constant while its intensity is increased from zero to H_{ext}. The forces F_N and F_S act on the length of the magnet to generate a torque

$$T_{mag} = q_m H_{ext} l_{mag} \sin(\gamma - \phi) \qquad (8)$$

The magnetic charge is given by $q_m = MA_{mag}$ with magnetization M and magnet cross-sectional area A_{mag}. Equation (8) thus reduces to

$$T_{mag} = V_{mag} M H_{ext} \sin(\gamma - \phi) \qquad (9)$$

where V_{mag} is the volume of the magnet.

As is familiar for a compass needle, an unrestrained magnetic element will rotate until it is aligned with the magnetic field ($\phi = \gamma$). However, if the rotation of the magnet is restrained by a mechanical spring, the magnetic torque T_{mag} causes the magnet to rotate until the mechanical restoring torque of the spring

$$T_{mech} = k_\phi \phi \qquad (10)$$

compensates for T_{mag} and an equilibrium angle is attained. The mechanical restoring torque that achieves

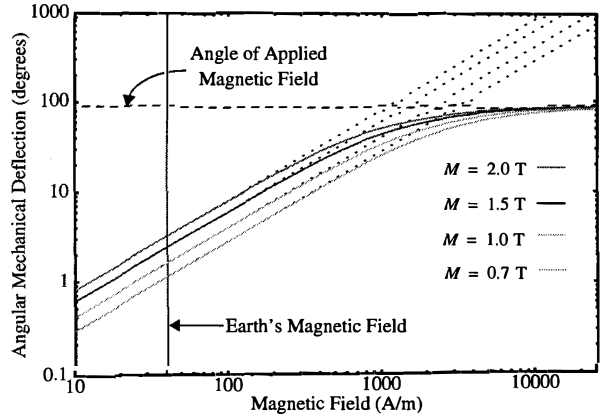

Fig. 5. Plot of the theoretical angular mechanical deflection ϕ as a function of magnetic-field intensity H_{ext}. The magnetization M is varied (0.7, 1.0, 1.5, and 2.0 T). The magnetic field is applied at a constant angle $\gamma = 90°$. The beam is made of polysilicon with an elastic modulus E_Y = 170 GPa and dimensions 2x2x400 μm^3 (k_ϕ = 567 pNm). The magnet has dimensions 10x100x400 μm^3.

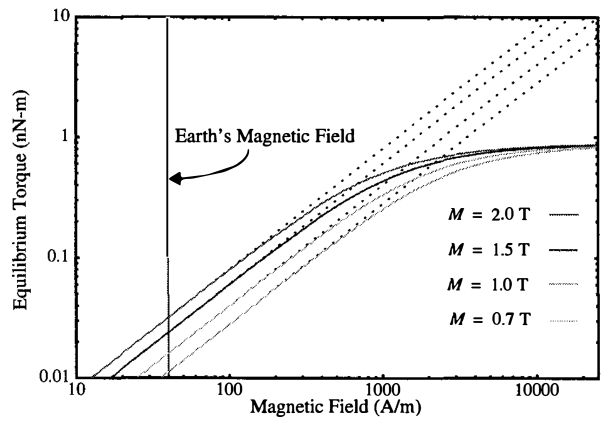

Fig. 6. Plot of the theoretical equilibrium torque for the same conditions used in Fig. 5.

equilibrium is referred to as the equilibrium torque T_{equil}. By equating Eqns. (9) and (10), the angular mechanical deflection of the cantilever structure is found

$$\phi = \left(\frac{V_{mag} M H_{ext}}{k_\varphi}\right) \sin(\gamma - \phi) \qquad (11)$$

Eq. (11) is a transcendental equation that can be solved numerically. Plots of the angular mechanical deflection ϕ and the equilibrium torque T_{equil}, as functions of magnetic-field intensity H_{ext}, are given in Figs. 5 and 6, respectively. In both plots, the lines reach asymptotic values defined by the choice for the direction of the stationary magnetic field ($\gamma = 90°$). If the relative angular difference between the magnet and the magnetic field is maintained at $\gamma - \phi = 90°$, the magnetic torque given in Eq. (9) is maximized. The extrapolated lines illustrate the maximum angular deflection and equilibrium torque possible for a given magnetic field. This occurs when the angle of the magnetic field is allowed to rotate with the moving magnet. The magnetic material was formed into rectangular and elliptical shapes to investigate the effects of shape on device performance. An ellipsoid is a special geometry for a magnetic material because an ellipsoid can

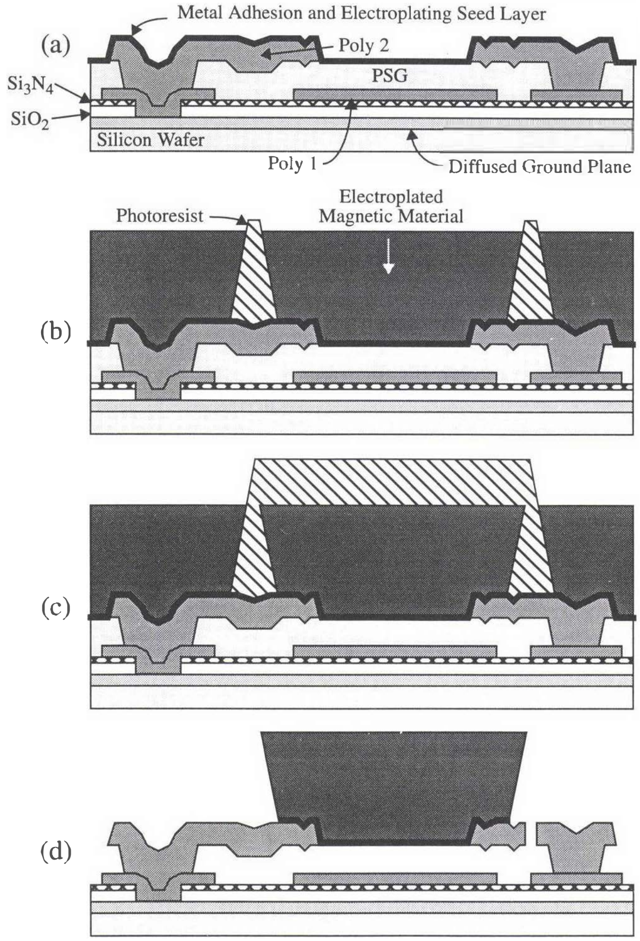

Fig. 7. (a) Metallic adhesion and seed-layer deposition. (b) Photoresist frame definition and magnetic-material electrodeposition. (c) Protective photoresist definition prior to magnetic-material etch. (d) Sacrificial material removal and fuse breaking to release the device.

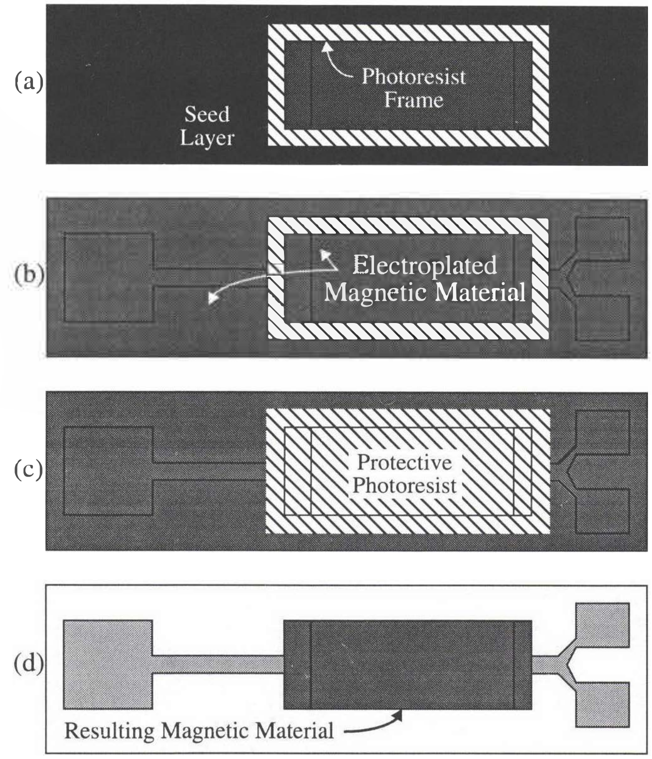

Fig. 8. Top view of the fabrication process which illustrates the frame plating technique. (a) Definition of a photoresist frame on top of the adhesion and seed layers. (b) Electrodeposition of the magnetic material. (c) Definition of the protective photoresist. (d) Removal of excess NiFe and protective photoresist.

be magnetized *uniformly* and the effect of its shape can be calculated analytically [15]. However, the magnetic theory described above is not appropriate for ellipsoids or rectangles that have aspect ratios (length/width) of less than ~4. This is because the magnetization vector inside the magnetic material can rotate away from the easy axis and thus the material no longer acts like a permanent magnet. All experimental data reported in this paper were obtained from actuators that had rectangular pieces of magnetic material with an aspect ratio of 10.

V. FABRICATION

As stated in Section II, magnetic elements were fabricated in steps added at the end of a process that had been developed to produce polysilicon resonant structures. With only the final "release" step for mechanical structures remaining, an adhesion layer (10 nm of Cr) and an electroplating seed layer (100 nm Cu) are deposited by evaporation on top of the polysilicon flexure (Fig. 7a).

Next, four layers of a common I-line photoresist (Olin Hunt 6512) are spun onto the wafer which aggregates to a total resist thickness of roughly 10 μm. The wafer is then exposed in an optical (10:1 reduction) wafer stepper (GCA) for 5.25 s per die. After developing the resulting photoresist, the sidewall slope is quite low (45 to 60°). Fortunately, abrupt vertical slopes on the resist are not important for these devices. This is because actuation by an external magnetic field does not require surface-to-surface interactions such as those found in linear and rotary variable-capacitance and variable-reluctance microactuators.

In the next step, the magnetic material is electroplated to a thickness of 7.0 μm (Fig. 7b). Because of the slope of the photoresist, the magnetic material has an inverted trapezoidal cross sectional. Except for the omission of a saccharin additive, the plating solution was the same as that described in reference [4]. To assure a uniform deposition rate and a uniform composition, a frame-plating technique is employed (Fig. 8b) [16]. After the thick resist is removed, a new layer is deposited and patterned over the regions of magnetic material that are to be preserved (Fig. 7c and Fig. 8c). The unprotected NiFe and the Cu beneath it are then removed. After the photoresist is stripped, the Cr adhesion layer is etched away in a dilute Cr etch (Fig. 8d). Unfortunately this etch results in a yield loss since the Cu is etched faster than the Cr and thus the NiFe becomes undercut. To improve yield a better method of removing the excess electroplating seed layer is needed. At this time, sputter etching and ion milling are being considered as alternatives. The devices are then released in a concentrated HF etch (Fig. 7d). Due to the

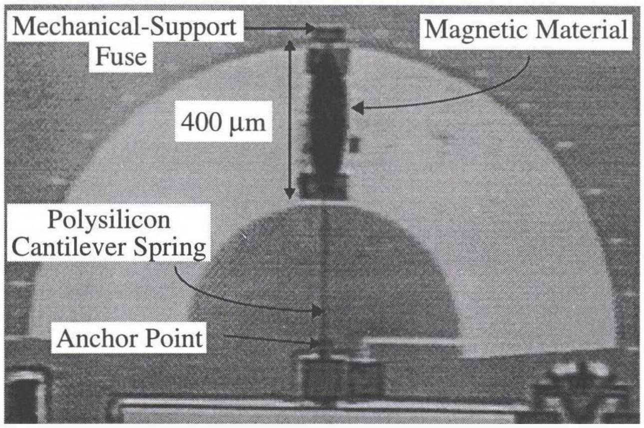

Fig. 9. Optical photograph of a microactuator with no applied magnetic field. This actuator consists of an elliptical piece of magnetic material with dimensions 400x(107-100)x7 μm^3 and a polysilicon beam with dimensions 400x(0.9-1.4)x2.25 μm^3.

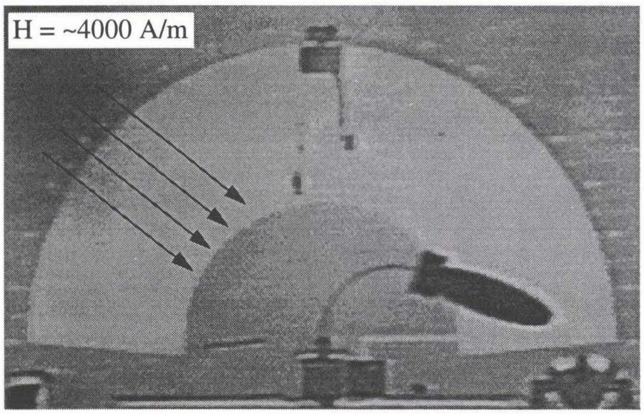

Fig. 10. Optical photograph of the microactuator with a large magnetic field applied at an angle γ greater than 90°.

large size and compliance of these devices, polysilicon fuses were used to help them survive the release etch and rinse [17].

VI. EXPERIMENTAL RESULTS

Figure 9 shows an optical photograph of one of the batch-fabricated magnetic microactuators when not under the influence of a magnetic field. Figure 10 shows the microactuator after it has been deflected by an applied magnetic field. For the purpose of illustration, the angle γ was allowed to increase beyond the nominal 90° to investigate the maximum deflection of these devices. A deflection greater than 180° was observed before the beam fractured.

Before we knew the composition of the NiFe film we had expected the material to demagnetize by breaking up into closure domains when the magnetic field was removed. Instead, it remained magnetized and hence acted like a permanent micromagnet. Since our films were nickel rich, such a permanent-magnet behavior is not surprising. The remanent magnetization can be overcome by applying a magnetic field that is larger than the coercive field. When the magnetization switches, the mechanical structure abruptly changes directions so that it points in a

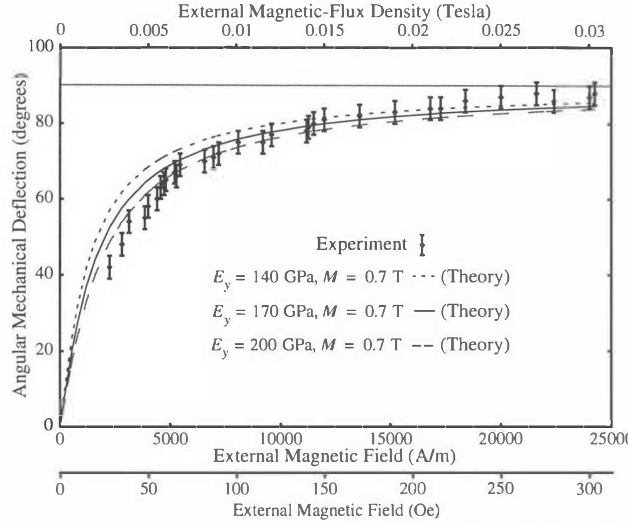

Fig. 11. Comparison of experimental deflection data and theoretical calculations for an actuator consisting of a rectangular piece of magnetic material with dimensions 400x(47-40)x7 μm^3 and a polysilicon beam with dimensions 400x(0.9-1.4)x2.25 μm^3.

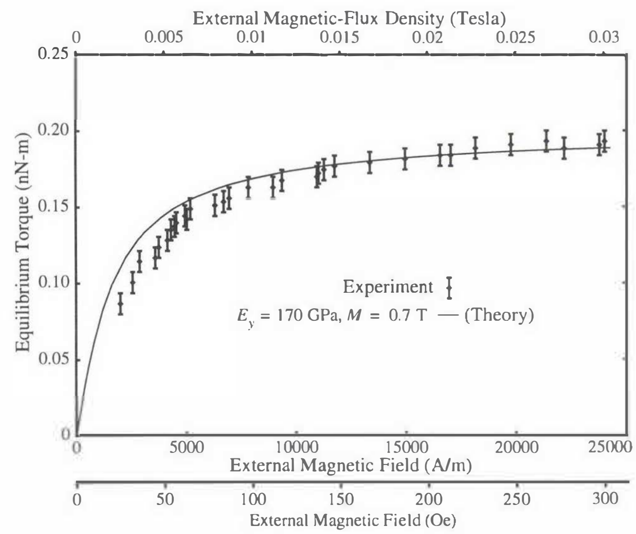

Fig. 12. Comparison of experimental torque data with theoretical calculations (k_ϕ = 127 pNm).

new equilibrium direction. Because of this observed permanent-magnet behavior, a more complex soft-magnetic material analysis is not required for these geometries [18].

The actuators were placed in a magnetic field created by an off-chip electromagnet. The magnetic field, which was varied from 0 to 24,000 A/m (300 Oe or 0.03 T), was maintained at a constant direction γ = 90° with respect to the original cantilever direction. The angular deflection of the device was measured optically. The measured angular deflections are compared with theory in Fig. 11. The theoretical curves give approximate bounds for variations of the elastic modulus E_Y of polysilicon. Using Eq. (2) the measured angular deflection is converted into an experimental torque which is then compared to the theoretical calculations obtained with E_Y = 170 GPa (Fig. 12). The experimental results agree well with the theoretical curves especially at higher magnetic fields.

There are two explanations for the over estimate at low magnetic fields. First, the magnetization M, which is assumed to be constant, is actually a hysteretic function of the applied magnetic field. The magnetization at low magnetic fields is lower than the magnetization at high fields. Second, the effective magnetic charges are assumed to be located at the very ends of the magnet. In practice the magnetic charges are distributed in a volume located near the ends of the magnet. The distance between the charge distributions is less than the physical length of the magnetic material. Therefore, the effective length of the magnet is shortened and the magnetic torque given by Eq. (8) is reduced.

The amount of mechanical force that can be applied by this microactuator is limited by the stiffness of the mechanical flexure. If the flexure is very compliant, then large deflections are possible. However, attempts to push a heavy object cause the beam to bend away from the object instead of transferring the force. If the mechanical flexure is made stiffer, the actuator is able to apply larger forces to an object, but the maximum displacement is reduced. Thus, for a given application, the desired torques, forces, and displacements determine the mechanical-flexure geometry, the magnetic-material geometry (volume and length-to-width aspect ratio), and the required magnetic field.

VII. CONCLUSIONS

This research has demonstrated that magnetic films can be integrated into surface micromachining with polysilicon microflexures. The tip of an 800 μm long cantilever has been deflected over a distance of 1.2 mm and rotated through an angle of >180° under an imposed torque of greater than 0.185 nNm. Actuation both in and out of the plane of the wafer is easily achieved. Similarly fabricated magnetically actuated microstructures might be applied to micromanipulators, microgrippers, magnetometers or microphotonic systems. Magnetic force is also of interest for studies of fundamental properties like yield and fracture strain as well as for crack propagation in polysilicon microstructures. Increasing the concentration of Fe from 5 to 50% should theoretically increase the magnetic torque at a given field by a factor of 2.0.

ACKNOWLEDGMENTS

The authors thank the staff of the Berkeley Microfabrication Laboratory for excellent support and service. We are grateful for helpful discussions with Prof. Jack H. Judy concerning magnetism and magnetic materials. In addition, the following members of the Recording Heads Department, Almaden Research Center, IBM Research Division were valuable resources of practical magnetic-materials-processing knowledge and advice: Long-Sheng Fan, Robert Fontana, Linda Lane, Tim Reiley, Neil Robertson, and Ching Tsang. Partial graduate-student research support was provided by an IBM Fellowship and by the State of California CALTRANS PATH project.

REFERENCES

[1] B. Wagner, W. Benecke, G. Engelmann, and J. Simon, "Microactuators with moving magnets for linear, torsional, or multiaxial motion," *Sensors and Actuators A (Physical)*, Vol. A32, no. 1-3, pp. 598-603, 1992.

[2] H. Guckel, K. J. Skrobis, T. R. Christenson, J. Klein, S. Han, B. Choi, E. G. Lovell, and T. W. Chapman, "Fabrication and testing of the planar magnetic micromotor," *J. Micromech. Microeng.*, vol. 1, no. 3, pp. 135-138, 1991.

[3] C. H. Ahn and M. G. Allen, "A fully integrated micromagnetic actuator with a multilevel meander magnetic core," *Tech. Dig. IEEE Solid-State Sensor and Actuator Workshop*, Hilton Head Island, South Carolina, June 22-25, 1992, pp. 14-18.

[4] C. H. Ahn, Y. J. Kim, and M. G. Allen, "A planar variable reluctance magnetic micromotor with fully integrated stator and wrapped coils," *Proc. IEEE Micro Electro Mechanical Syst.*, Fort Lauderdale, Florida, February 7-10, 1993, pp. 1-6.

[5] H. Guckel, T. R. Christenson, H. J. Skrobis, T. S. Jung, J. Klein, K. V. Hartojo, and I. Widjaja, "A first functional current excited planar rotational magnetic micromotor," *Proc. IEEE Micro Electro Mechanical Syst.*, Fort Lauderdale, Florida, February 7-10, 1993, pp. 7-11.

[6] R. Brennen, A. P. Pisano, and W. C. Tang, "Multiple mode micromechanical resonators," *Proc. IEEE Micro Electro Mechanical Syst.*, Napa Valley, California, February 11-14, 1990, pp. 9-14.

[7] M. W. Judy and R. T. Howe, "Highly compliant suspensions using sidewall beams," *7th Int. Conf. Solid-State Sensors and Actuators Dig. of Tech. Papers*, Yokohama, Japan, June 7-10, 1993, pp. 54-57.

[8] N. Takeshima, K. J. Gabriel, M. Ozaki, J. Takahashi, H. Horiguchi, and H. Fujita, "Electrostatic parallelogram actuators," *7th Int. Conf. Solid-State Sensors and Actuators Dig. of Tech. Papers*, Yokohama, Japan, June 7-10, 1993, pp. 63-66.

[9] W. C. Tang, T.-C.H. Nguyen, M. W. Judy, and R. T. Howe, "Electrostatic-comb drive of lateral polysilicon resonators," *Sensors and Actuators A (Physical)*, vol. A21, no. 1-3, pp. 328-331, 1990.

[10] R. Bozorth, *Ferromagnetism*, New York, D. Van Nostrand Company Inc., 1951. (Reprinted 1978 AT&T, New Jersey)

[11] *Energy-Dispersive X-Ray Microanalysis: An Introduction*, Kevex Corporation, Foster City, California 94404, 1983.

[12] B. D. Cullity, *Introduction to Magnetic Materials*, Reading, Massachusetts, Addison-Wesley Pub. Co., 1972, p. 527.

[13] E. P. Popov, *Engineering Mechanics of Solids*, Englewood Cliffs, New Jersey, Prentice Hall, 1990.

[14] R. J. Roark, *Roark's Formulas for Stress and Strain*, Warren C. Young, Editor, New York, McGraw-Hill, 1989.

[15] J. A. Osborn, "Demagnetizing factors of the general ellipsoid," *Phys. Rev.*, vol. 67, no. 11 & 12, pp. 351-357, 1945.

[16] S. Liao, "Electrodeposition of magnetic materials for thin-film heads," *IEEE Transactions on Magnetics*, vol. 26, no. 1, pp. 328-332, 1990.

[17] G. K. Fedder, J. C. Chang, and R. T. Howe, "Thermal assembly of polysilicon microstructures with narrow-gap electrostatic comb drive," *Tech. Dig. IEEE Solid-State Sensor and Actuator Workshop*, Hilton Head Island, South Carolina, June 22-25, 1992, pp. 63-68.

[18] J. W. Judy, "Magnetic microactuators with polysilicon flexures," *Masters Report*, Department of Electrical Engineering and Computer Sciences, University of California, Berkeley, 1994.